10th International Conference on
Steel and Aluminium Structures (ICSAS24)
Rio de Janeiro, Brazil, 5-7, June, 2024

INSIGHTS INTO THE CYCLIC BEHAVIOUR OF NOVEL HYBRID INTER-MODULE JOINTS UNDER LATERAL LOAD

Konstantinos Daniel TSAVDARIDIS[a] and Dan-Adrian CORFAR[a]

[a] Department of Engineering, School of Science & Technology, City, University of London, London, UK
Email: Konstantinos.Tsavdaridis@city.ac.uk

Keywords: Steel modular buildings; Inter-module joints; Rubber bearings; Cyclic load; Low damage; Disassembly and reuse.

Abstract. *Three cyclic tests with bi-axial loading were carried out on meso-scale inter-module joint assemblies using a novel hybrid inter-module connection with high-strength steel bolts and rubber bearings in order to determine the mechanical behaviour of the proposed connection at joint level. The tests also included different intra-module connection details and bolt sizes. The results showed that all three hybrid IMJs displayed nonlinear hysteretic responses, while the presence of stiffeners at the intra-module connection and the larger bolt size had a favourable effect on the failure mode, lateral load capacity and stiffness degradation of the joints. According to Eurocode 3, the hybrid joints were classified as semi-rigid, partial strength in terms of stiffness and strength respectively. Furthermore, the strain analysis results demonstrated the feasibility of the proposed connection with respect to the limitation of damage in the structural elements of the volumetric under cyclic lateral load, improving the reclaim and reuse potential of the module.*

1 INTRODUCTION

The past two decades have known rapid advancements in Off-site Manufacturing (OSM) and Off-site Construction (OSC) driven by the need to address the housing crises around the globe while at the same time minimising the negative impact of the construction industry on the environment [1,2]. While the development of modern methods of construction (MMC) has reinforced the already proven benefits of prefabrication and standardisation regarding resource efficiency [3–6], the Design for Manufacture and Assembly (DfMA) and Design for Deconstruction (DfD) principles at the core of steel modular building systems (MBSs) have drawn the spotlight on the technology's potential to implement the circular economy design philosophy in the built environment [7–10].

In this context, the design of connections between the volumetric modules (or inter-module connections - IMCs) is paramount for the demountability and adaptability of steel modular buildings due to their discretised nature with multiple connection points at the interfaces of stacked or adjacent volumetrics. Moreover, the role of inter-module connections becomes critical in the behaviour of tall self-standing steel modular buildings under lateral load [11–14], while current practice often compromises on demountability in favour of frame continuity by adopting welded or grouted joints between modules [15]. As such, significant effort has been devoted to the adoption of capacity design from traditional steel moment-resisting frames (MRFs) to steel MBSs by designing inter-module joints to perform elastically while plastic hinges are formed in the beams of the modular frame [16–19]. Although efficient in terms of life safety, this design paradigm results in large residual deformation which reduces the

functionality and ease of disassembly of the steel modular building in the aftermath of an earthquake, while the significant permanent damage to the members of the volumetric renders its reusability credentials impractical.

Thus, in view of the need for improved sustainability and resilience of the built environment emphasised by the United Nations' Sustainable Development Goals (SDGs) [20,21], there has been increasing interest among researchers in the topic of resilient steel modular buildings, with a focus on a new generation of inter-module connections which contribute effectively to the global damage distribution mechanism of modular structures by employing various energy-dissipating and self-centring parts in their configuration [22–28]. In this respect, the authors have recently proposed a novel hybrid IMC designed to reduce the permanent damage in the volumetric by means of laminated elastomeric bearings inserted between the modules and explored its mechanical behaviour under cyclic load at connection level through validated proof-of-concept finite element analysis, reporting promising re-centring and damage control capabilities [29].

In this paper, the in-plane cyclic behaviour of inter-module joints assembled with the hybrid connection was investigated in order to determine the feasibility of the proposed IMC at joint level. The tests were carried out on meso-scale prototypes with full-size members to highlight the efforts developed in the volumetric framing elements during the deformation stages of a FEMA/SAC loading sequence.

2 DETAILS OF THE PROPOSED HYBRID CONNECTION

Figure 1 shows the schematic of the proposed inter-module connection. The connection has been designed to ensure vertical and horizontal connectivity between modules, while the centred alignment of the member cross-sections to the box corners eliminates the unfavourable effect of eccentric loads caused by offsets. Axial compression is transferred between the corner posts through the laminated elastomeric bearing made with steel reinforcing plates to control the level of vertical displacement, whereas tensile axial force would be resisted by the bolting assembly. Horizontal shear forces are transferred through a combined mechanism of friction between the faying steel surfaces, shear resistance of the rubber bearing, and bending of the bolt rod, while the interlocking pins prevent accidental sliding.

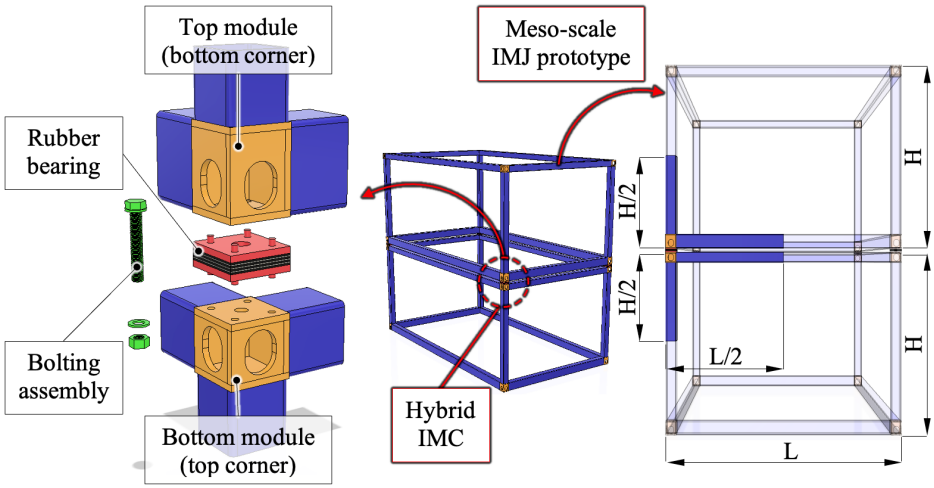

Figure 1: Graphical illustration of the hybrid inter-module connection

To improve the energy dissipation capacity of the rubber bearing at the shear deformation levels expected in the IMC (50%-100% shear strains), the rubber layers were made of high-

damping (filled) rubber instead of low-damping (unfilled) rubber, as the addition of carbon black filler improves the hysteresis of rubber [30,31].

3 DETAILS OF THE CYCLIC TESTS

3.1 Configuration of test prototypes

The inter-module joint prototypes were designed based on the meso-scale configuration shown in Figure 1, adopted for its cost-effectiveness. This solution replicates the deformed shape and anticipated points of inflection in planar modular frames subjected to in-plane lateral loads by limiting the lengths of the column and beams to half of those in the full-size frame panel. As summarised in Table 1, three prototypes were considered for the cyclic tests to determine the effect of the bolt size and stiffness of the intra-module connection on the mechanical behaviour of the hybrid IMJs under lateral load.

Table 1: Inter-module joint specimens

Joint specimen ID	Bolt size	Intra-module connection
JS-1	M24	No stiffeners
JS-2	M24	With stiffeners
JS-3	M27	With stiffeners

The meso-scale prototypes consisted of T-shaped frames assembled from beam-column subassemblages representing the top and bottom corners of lower and upper modules respectively, stacked on top of each other and connected by means of the hybrid inter-module connection with a laminated elastomeric bearing and bolting assembly. The beam-column subassemblages (Figure 2) were made of S355J2H steel cold-formed hollow members, joined to S355J2H steel-plated box corner fittings by complete joint penetration (CJP) groove welds. The box corner fittings were fabricated from 15-mm-thick steel plates. Two S355J2H steel stiffeners of 100 mm x 100 mm x 10 mm triangular plate were welded at the beam-column connection for specimens JS-2 and JS-3.

The laminated elastomeric bearings (Figure 3) were fabricated with two outer S355 steel plates (150 mm x 150 mm x 15 mm), four high-damping rubber layers (150 mm x 150 mm x 4 mm) and three steel shims (150 mm x 150 mm x 3 mm), designed to achieve a shape factor of S = 8.85 to improve the stability of the bearing and limit the bulging of the rubber layers under the applied axial load. The bolting assemblies consisted of standard full-thread hexagon head bolts made of class 8.8 high-strength steel (HSS). The two bolt sizes shown in Figure 4 were M24 x 150mm for specimens JS-1 and JS-2 and M27 x 120 mm for specimen JS-3.

The mechanical properties of the structural steel used in the members of the T-frames and the high-damping rubber compound in the layers of the laminated elastomeric bearing were obtained from material characterisation tests and were given in Table 2 and Table 3 respectively.

Table 2: Material properties of structural steel

Frame member	Steel grade	Young's modulus	Yield strength	Ultimate tensile strength	Elongation percent after fracture
Top post	S355J2H	209 GPa	505 N/mm^2	546 N/mm^2	28.2 %
Bottom post	S355J2H	205 GPa	438 N/mm^2	496 N/mm^2	30.9 %
Floor beam	S355J2H	190 GPa	433 N/mm^2	507 N/mm^2	32.4 %
Ceiling beam	S355J2H	202 GPa	541 N/mm^2	565 N/mm^2	19.5 %

Table 3: Material properties of the high-damping rubber

Hardness[a]	Shear modulus, G[c]	Effective damping ratio, $\xi_{eff,b}$[c]
86 IRHD[b]	0.61 MPa	18.46 %

[a] based on shear modulus at 5% shear strain, [b] International rubber hardness degree, [c] at 100% shear strain

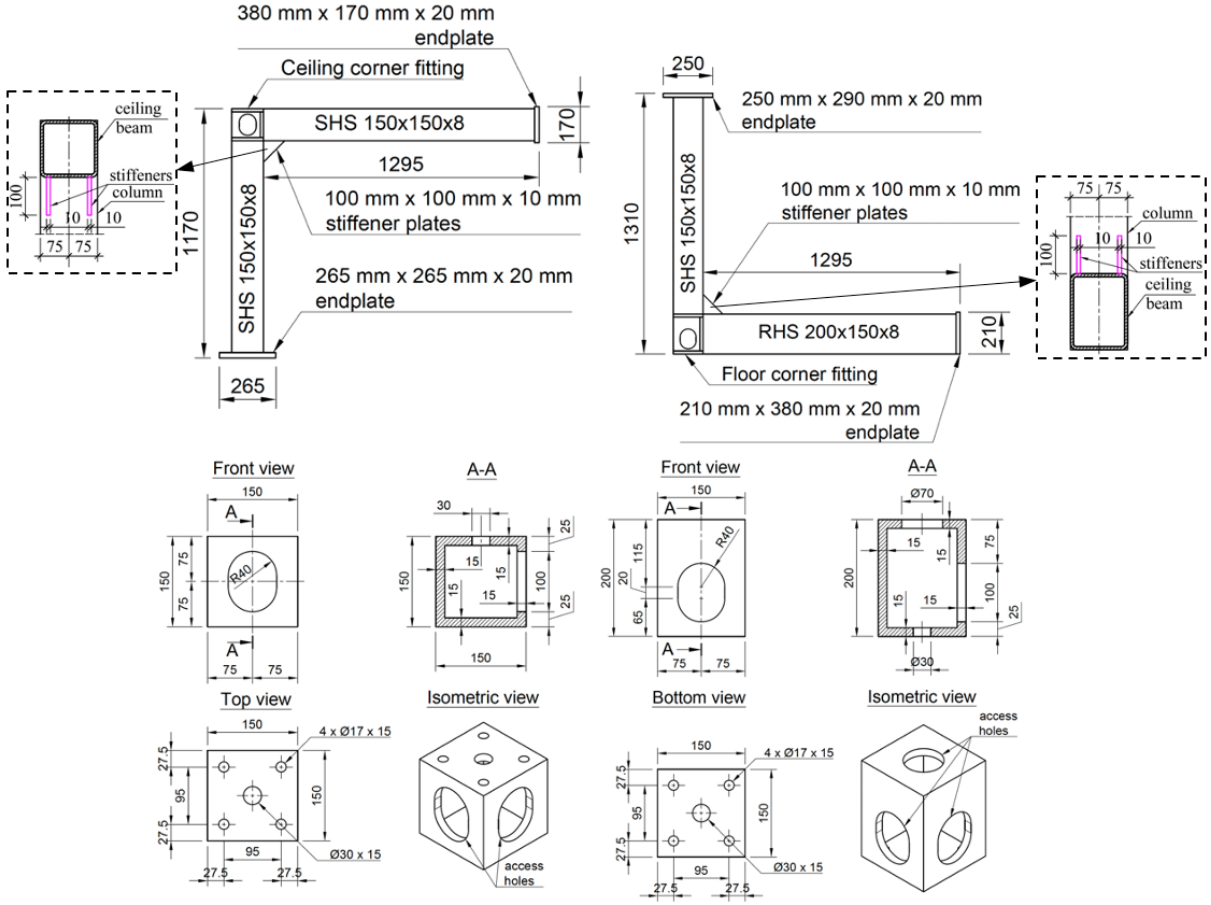

Figure 2: Details of the beam-column subassemblages (shown for stiffened samples)

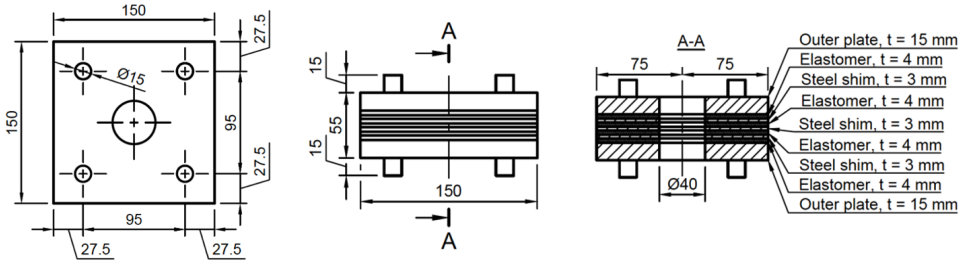

Figure 3: Details of the laminated elastomeric bearings

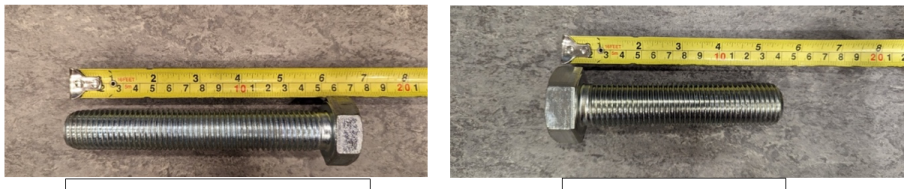

M24 x 150 mm (JS-1 and JS-2) | M27 x 120 mm (JS-3)

Figure 4: High-strength steel bolts

3.2 Test setup and loading protocol

Figure 5 shows a diagram of the test frame and its loading system, designed to simulate the appropriate support conditions for the IMJ prototypes under the effect of bi-axial loading applied to the top column, according to the J/C test setup for unbraced modular frames subjected to lateral load [32]. The tests were carried out according to the ANSI/AISC 341-22 [33] recommendations, while the displacement-controlled standard FEMA/SAC [34] loading sequence given in Table 4 was applied through the horizontal actuators in a quasi-static manner at a rate of 10mm/min to limit the influence of dynamic effects. To capture the effect of gravitational actions, an axial load equivalent to 5% of the compressive yield capacity of the 150x150x8 SHS post and 4.7 MPa compressive stress on rubber bearing was kept constant throughout the test. The instrumentation layout was shown in Figure 6.

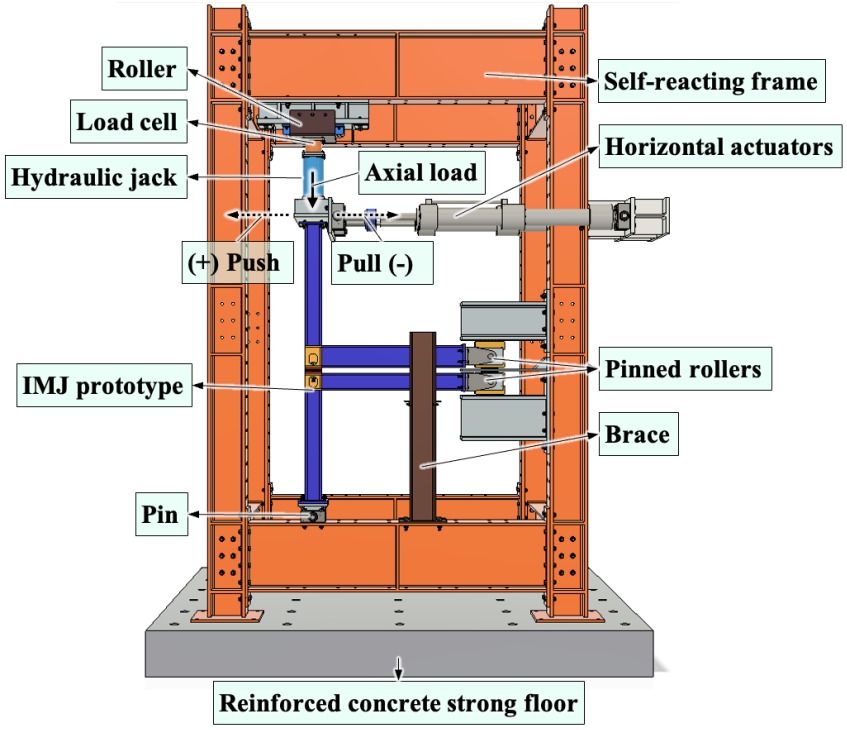

Figure 5: Diagram of the test apparatus and the loading system

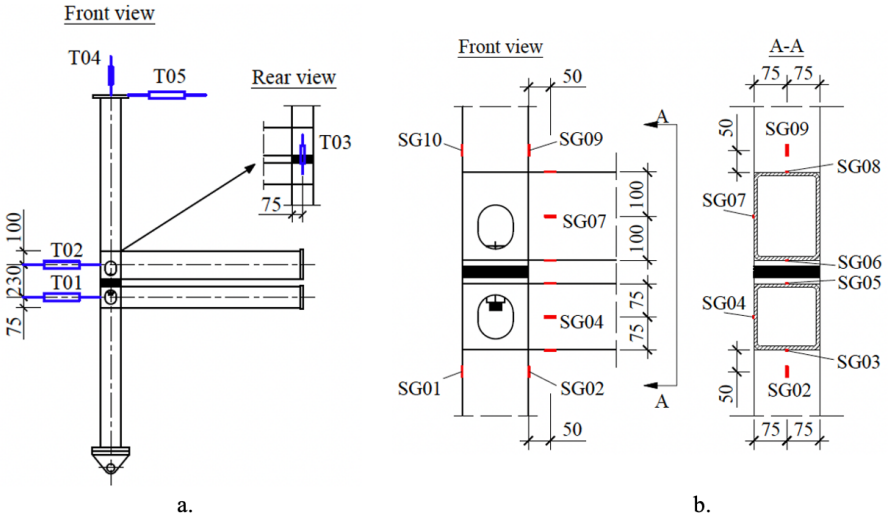

a. b.

Figure 6: Location of potentiometers (a) and strain gauges (b)

Table 4: Cyclic test protocol based on FEMA/SAC loading history

Loading stage	Inter-storey drift ratio	Applied lateral displacement	Number of cycles
1	0.375%	10.3 mm	6
2	0.5%	13.8 mm	6
3	0.75%	20.6 mm	6
4	1%	27.5 mm	4
5	1.5%	41.3 mm	2
6	2%	55 mm	2
7	3%	82.5 mm	2
8	4%	110 mm	2

4 RESULTS OF THE CYCLIC TESTS

4.1 Test observations and hysteretic curves

The three test prototypes completed the 30 cycles planned for the lateral load protocol with similar overall stiffness and lateral load capacity up to 3% drift ratio, while the impact of the intra-module connection stiffeners and bolt diameter was more evident during the 4% drift ratio cycles. The hysteresis loops of the three specimens were characterised by a reverse S shape and high nonlinearity with low strength and stiffness during the low-amplitude cycles owing to the governing role of the rubber bearing during the early stages of deformation.

At the peak lateral displacement reached during the first 4% drift ratio cycle, specimen JS-1 reached a maximum lateral load capacity of 63 kN in the positive loading direction and 73 kN in the negative direction (see Figure 7). After the peak was reached in the positive loading direction during the second ±4% drift ratio cycle, the fillet weld at the ceiling beam-column connection cracked, causing the peak lateral load in the reverse direction to fall to 62 kN (85% of the previous maximum). Thus, the controlling failure mode was identified as the weakened beam-column connection, which was in good agreement with results from similar tests [35–37], emphasising the need to provide stiffeners at the intra-module connection to ensure it performed elastically and avoid premature damage. Out of the three tests, specimen JS-1 experienced the most noticeable bending deformation in the M24 HSS bolt at the end of the load protocol.

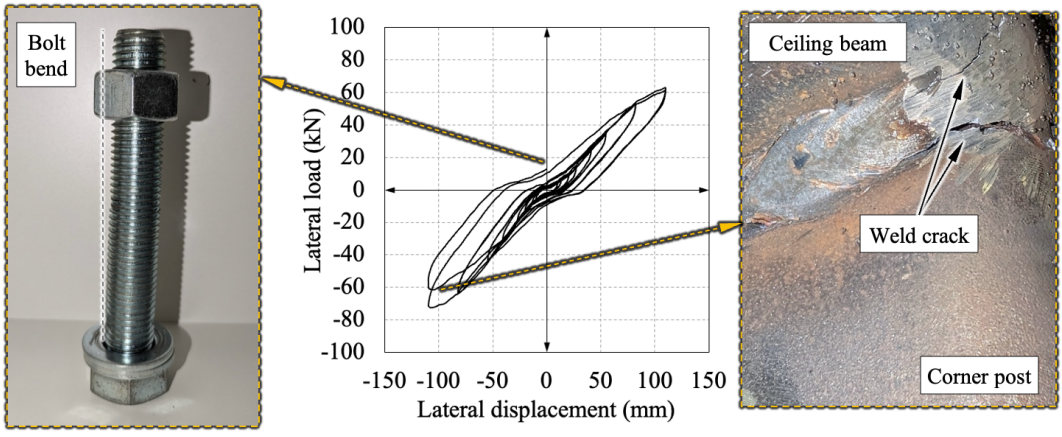

Figure 7: The hysteretic curve of specimen JS-1

The bend of the M24 HSS bolt from specimen JS-2 was comparable to that observed in specimen JS-1, which was expected since both specimens had the same bolt diameter. The main

difference in the load-displacement behaviour was provided by the two stiffener plates welded at the beam-column connection of the subassemblages, which resulted in 9% larger lateral load capacity in the negative loading direction (80 kN) and no noticeable damage to the welds at the intra-module connection. In the positive loading direction, the specimen reached 66 kN lateral load capacity, yet a malfunction of the control system caused the two actuators to enter load reversal before reaching the peak lateral displacement corresponding to 4% drift ratio. Nevertheless, the results from the other two tests suggested that the lateral load capacity corresponding to the 4% drift ratio would have been very close to the 66 kN value obtained, supporting the validity of the present result.

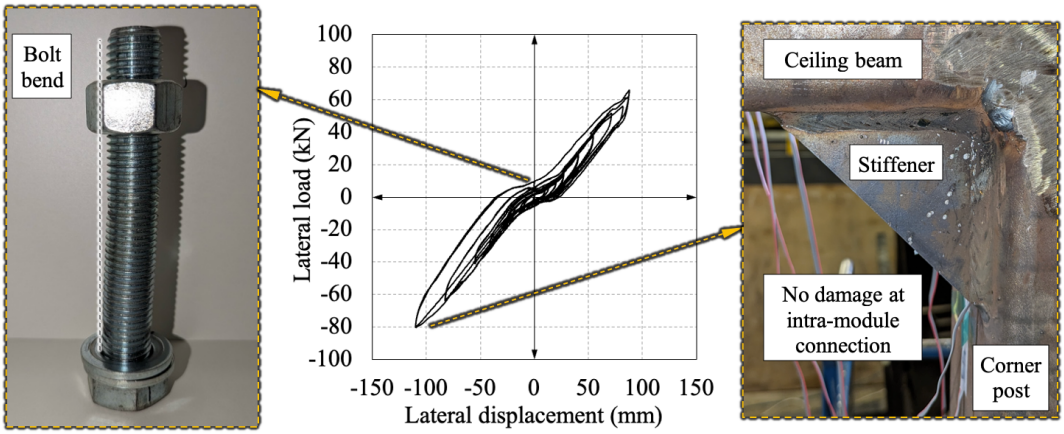

Figure 8: The hysteretic curve of specimen JS-2

Similarly, specimen JS-3 recorded a lateral load capacity of 69 kN in the positive loading direction and 84 kN in the negative loading direction, outperforming specimen JS-1 by 7% and 13% respectively. The specimen completed the full 30 cycles of the FEMA/SAC protocol without any damage to the beam-column connections or framing members, while the deformation of the bolting assembly was even less noticeable due to the larger diameter of the M27 bolt. The effect of the bigger HSS bolt size was also reflected by the 5% larger lateral load capacity when compared to the result of specimen JS-2.

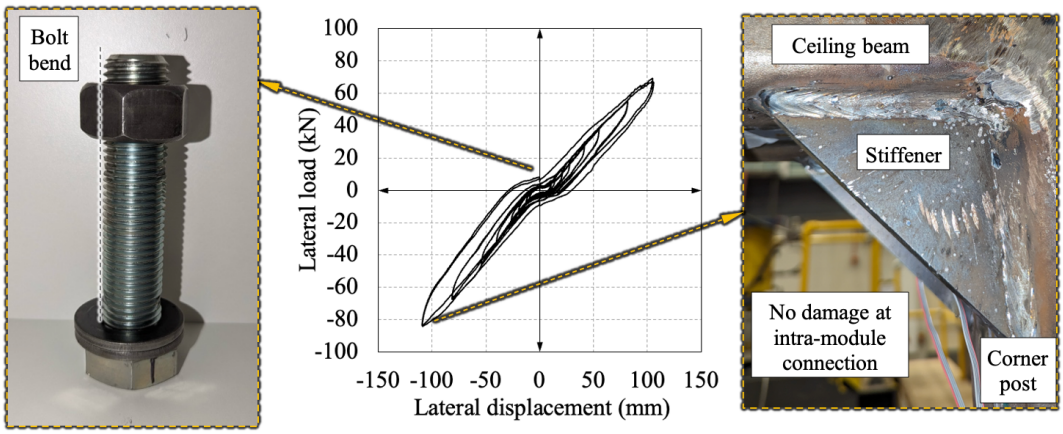

Figure 9: The hysteretic curve of specimen JS-3

4.2 Stiffness and strength characteristics

Figure 10a illustrated the stiffness and strength classification of the hybrid IMJs according to Eurocode 3, Part 1-8 [38], based on the plastic section properties of the 150 mm x 150 mm x 8 mm SHS ceiling beam and the material properties of the S355 steel given in Table 2. As per

the boundaries defined by Eurocode 3, the hybrid inter-module joints were classified as semi-rigid from the point of view of stiffness characteristics and partial-strength from the point of view of strength classification, reflecting the need to consider explicitly the nonlinear behaviour of the joints in global analysis models. The values of the bending moment in the ceiling beam, M_{cb}, were assumed to be equal to the bending moment in the bottom column and were determined as the product of the horizontal reaction at the bottom pin support (equal to the lateral load applied at the top) and the distance to the face of the ceiling beam (1140 mm). The values were further adjusted by the P-delta effect resulting from the 100 kN axial load and the corresponding horizontal displacement recorded by transducer T01 shown in Figure 6.

Figure 10b showed the stiffness degradation, taken as the ratio of the initial secant stiffness at 0.375% drift ratio to the secant stiffness corresponding to subsequent drift ratios. The results exhibited rapid stiffness changes during the small amplitude cycles in both loading directions due to the stress-softening of the high-damping rubber and the partially loose state of the bolt assemblies, which experienced various movements allowed by the bolt hole clearance during these early stages. After the 1% drift ratio level, the overall stiffness of the connections increased steadily, owing to the increasing contribution of the frame members as all bolt assemblies were engaged completely by the shear deformation of the bearings at this stage, peaking during the 2% drift ratio cycle. Overall, the samples demonstrated a remarkable performance with limited degradation rates in both loading directions, emphasising the effectiveness of the hybrid IMC in hindering the cumulative damage in the joints. In particular, specimen IMJ06 outperformed the others by finishing the test with a 20% stiffness increase, showcasing the favourable influence of the M27 HSS bolt and stiffened intra-module connections.

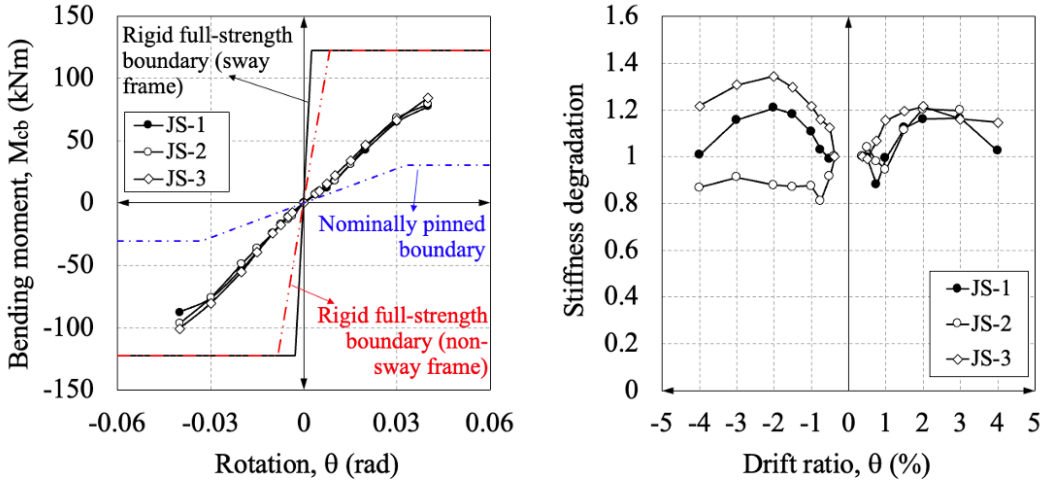

Figure 10: Stiffness evaluation of the hybrid IMJs

4.3 Strain response

The strain vs. displacement curves reflected the cyclic behaviour of the hybrid joints from a material level perspective, illustrating the distribution of effort between the framing members of the joint. The yield strain was taken as 0.00437 based on the average of the yield strains obtained from the tensile coupon tests, where the corresponding yield strength was taken as the proof strength at 0.2% strain offset in lack of a flat yield plateau. Due to operational issues during the test on specimen JS-1, readings from gauges SG01, SG04, SG07, and SG10 were not available.

Figure 11 showed the expected strain distribution in the beams, with larger values in the top and bottom flanges of the hollow profiles and almost negligible strain levels near the neutral axes (SG04 and SG07). Up to 3% drift ratio, the beams strain values were less than 50% of the yield strain in all three specimens, oscillating around 2000 microstrains. Unsurprisingly, the outer flanges in the two beams (SG03 and SG08) recorded higher strains than the inside flanges (SG05 and SG06), attributed to the increased stresses in the stiffer regions closest to the intra-module connection. Moreover, the presence of stiffeners at the beam-column joint caused a steep surge in the strains, observed after the 3% drift ratio level, highlighting the greater influence of the intra-module connection stiffness on the cyclic behaviour of the IMJs during the third stage of deformation.

Similarly, it was observed that the column strains fluctuated below the yield strain up to 4% drift ratio (see Figure 12), with the notable exception of JS-3 in which the inside flanges reached almost twice the yield strain at the 4% drift ratio in the negative loading direction. However, as the strains of the outside flanges of the column (SG01 and SG10) were generally much lower than the strains on the inside flanges (SG02 and SG09), it may be assumed that the higher strain values were a result of a stress concentration between the two stiffener plates. This effect was further supported by the results of specimen JS-1, which exhibited comparable strain values between both sides of the beam and column flanges, regardless of the direction of loading.

Overall, the strain results demonstrated the damage control capability of the hybrid connection which minimised the effort in the connecting members of the joint. This was mainly explained by the key role of the rubber bearing in the cyclic behaviour of the joints, characterised by the sequential activation of the connection components at different deformation levels which delayed the full contribution of the steel frame members until the large amplitude cycles. It must be noted that the current assessment was based on the yield strain determined from the steel coupon tests. When compared to the yield strain from nominal material properties of S355 steel (ca. 1690 microstrains), it may be judged that the yield of the beams and columns occurred between the 2% and 3% drift ratio levels, highlighting the need for careful consideration of overconservative design values when selecting the steel grade to meet the desired yield strain limit in the volumetric.

The higher inelastic strains observed in specimen JS-2 and JS-3 revealed the effect of the size of the bolting assembly in the design of the IMC, as increasing the strength and stiffness of the hybrid connection causes larger efforts developed in the volumetric frame. Hence, the effectiveness of the proposed connection requires a fine balance between the design of each component in order to ensure the hybrid IMC can resist the forces transferred between the modules, without fully engaging the volumetric early on and damage its framing elements beyond practical repairability.

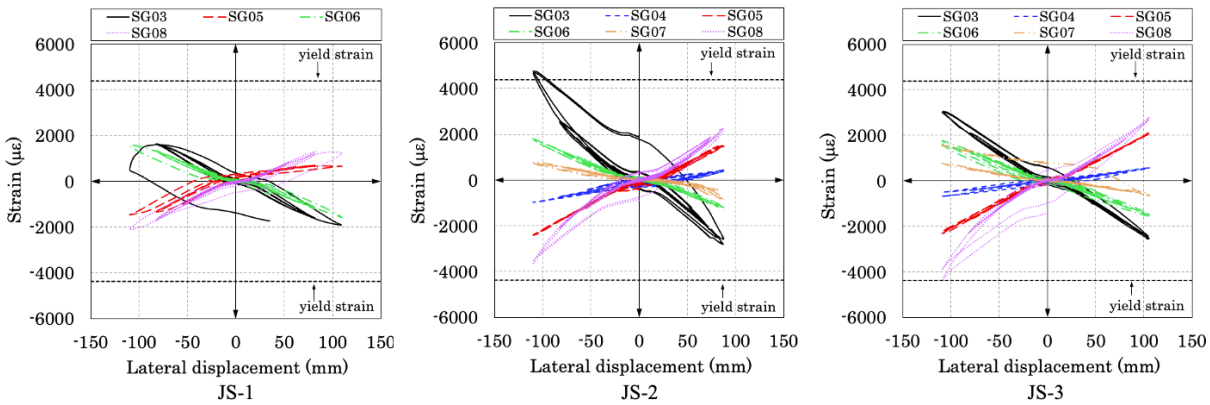

Figure 11: The values of strains in the beams

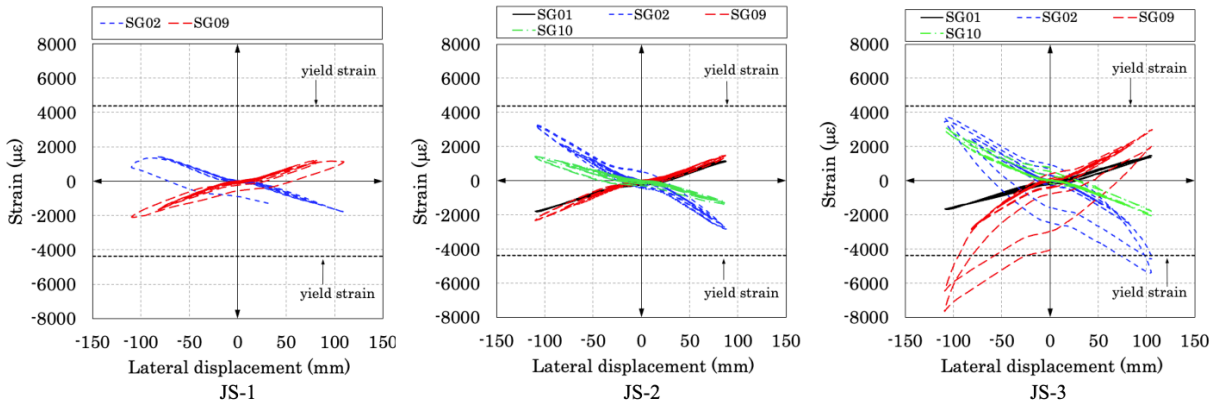

Figure 12: The values of strains in the columns

5 CONCLUSIONS

This study investigated the in-plane lateral load performance of inter-module joints equipped with a novel hybrid inter-module connection which employed a rubber bearing and high-strength steel bolts. Three tests were carried out on meso-scale joint assemblies with full-size members, including different beam-column connection details and bolt sizes.

The results reflected a nonlinear behaviour characterised by reverse S-shaped hysteresis loops in all three tests, while the presence of stiffeners at the intra-module connection and the larger bolt size had a favourable effect on the failure mode, lateral load capacity and stiffness degradation of the joints. Despite the prominent bends in the bolts, the two stiffened specimens completed the cyclic load protocol without noticeable effects on the lateral load capacity. The stiffness and strength classification revealed that all three IMJs performed as semi-rigid, partial-strength joints and their nonlinear behaviour should be modelled in global analysis.

The strain analysis showed that the joint members suffered limited plastic deformations throughout the 30-cycle protocol, with peak beam and column strains fluctuating around 2000 microstrains (50% of yield strain) up to 3% drift ratio. Ideally, the shear flexibility of the rubber bearing would generate a sequential activation of the connection components at different deformation levels, ensuring the lateral resistance of the joint while minimising the effort in the frame elements. The larger plasticity developed in the beams and columns of specimens JS-2 and JS-3 owing to the stiffened intra-module joint and larger bolt size reflected the design accuracy required to achieve the fine interplay between the strength and stiffness of each joint component to ensure the effectiveness of the hybrid IMC.

Thus, the cyclic tests demonstrated the feasibility of the proposed connection with respect to the limitation of damage in the steel frame under cyclic lateral load, improving the reclaim and reuse potential of the volumetric module. Future work should focus on developing simplified joint models for the hybrid IMC to investigate its effect on the global behaviour of steel MBSs and optimise the connection's design based on specific performance objectives.

REFERENCES

[1] Zhang R, Zhou ASJ, Tahmasebi S, Whyte J. Long-standing themes and new developments in offsite construction: the case of UK housing. Proceedings of the Institution of Civil Engineers - Civil Engineering 2019;172:29–35. https://doi.org/10.1680/jcien.19.00011.

[2] Steinhardt D, Manley K, Bildsten L, Widen K. The structure of emergent prefabricated housing industries: a comparative case study of Australia and Sweden. Construction Management and Economics 2019;38:483–501. https://doi.org/10.1080/01446193.2019.1588464.

[3] Gibb A. Off-site Fabrication: Prefabrication, Preassembly and Modularisation. Scotland: Whittles Publishing; 1999.

[4] Ferdous W, Manalo A, Sharda A, Bai Y, Ngo TD, Mendis P. Construction Industry Transformation Through Modular Methods. In: Ghaffar SH, Mullett P, Pei E, Roberts J, editors. Innovation in Construction, Cham: Springer; 2022, p. 259–76. https://doi.org/10.1007/978-3-030-95798-8_11.

[5] Gunawardena T, Mendis P. Prefabricated Building Systems—Design and Construction. Encyclopedia 2022;2:70–95. https://doi.org/10.3390/encyclopedia2010006.

[6] Lawson RM, Ogden RG, Goodier C. Design in Modular Construction. Oxon: CRC Press; 2014.

[7] McConnell JR, Fahnestock LA. Innovations in Steel Design: Research Needs for Global Sustainability. Journal of Structural Engineering 2015;141:02514001. https://doi.org/10.1061/(ASCE)ST.1943-541X.0001185.

[8] Minunno R, O'Grady T, Morrison GM, Gruner RL. Exploring environmental benefits of reuse and recycle practices: A circular economy case study of a modular building. Resources, Conservation and Recycling 2020;160. https://doi.org/10.1016/j.resconrec.2020.104855.

[9] Iacovidou E, Purnell P, Tsavdaridis KD, Poologanathan K. Digitally enabled modular construction for promoting modular components reuse: A UK view. Journal of Building Engineering 2021;42:102820. https://doi.org/10.1016/j.jobe.2021.102820.

[10] Sajid ZW, Ullah F, Qayyum S, Masood R. Climate Change Mitigation through Modular Construction. Smart Cities 2024;7:566–96. https://doi.org/10.3390/smartcities7010023.

[11] Lacey AW, Chen W, Hao H, Bi K. Effect of inter-module connection stiffness on structural response of a modular steel building subjected to wind and earthquake load. Engineering Structures 2020;213. https://doi.org/10.1016/j.engstruct.2020.110628.

[12] Wang Z, Tsavdaridis KD. Optimality criteria-based minimum-weight design method for modular building systems subjected to generalised stiffness constraints: A comparative study. Engineering Structures 2022;251:113472. https://doi.org/10.1016/j.engstruct.2021.113472.

[13] Wang Z, Rajana K, Corfar D-A, Tsavdaridis KD. Automated minimum-weight sizing design framework for tall self-standing modular buildings subjected to multiple performance constraints under static and dynamic wind loads. Engineering Structures 2023;286:116121. https://doi.org/10.1016/j.engstruct.2023.116121.

[14] Farajian M, Sharafi P, Eslamnia H, Kildashti K, Bai Y. Classification of inter-modular connections for stiffness and strength in sway corner-supported steel modular frames. Journal of Constructional Steel Research 2022;197:107458. https://doi.org/10.1016/j.jcsr.2022.107458.

[15] Corfar D-A, Tsavdaridis KD. A comprehensive review and classification of inter-module connections for hot-rolled steel modular building systems. Journal of Building Engineering 2022;50:104006. https://doi.org/10.1016/j.jobe.2022.104006.

[16] Dai X-M, Zong L, Ding Y, Li Z-X. Experimental study on seismic behavior of a novel plug-in self-lock joint for modular steel construction. Engineering Structures 2019;181:143–64. https://doi.org/10.1016/j.engstruct.2018.11.075.

[17] Chen Z, Wang J, Liu J, Khan K. Seismic behavior and moment transfer capacity of an innovative self-locking inter-module connection for modular steel building. Engineering Structures 2021;245:112978. https://doi.org/10.1016/j.engstruct.2021.112978.

[18] Zhai S-Y, Lyu Y-F, Cao K, Li G-Q, Wang W-Y, Chen C. Seismic behavior of an innovative bolted connection with dual-slot hole for modular steel buildings. Engineering Structures 2023;279:115619. https://doi.org/10.1016/j.engstruct.2023.115619.

[19] Yang C, Chen H, Wen H, Wang Q, Zhang B, Ou J. Experimental study on seismic performance of internal cruciform joints of grouting sleeve connection for modular integrated construction. Engineering Structures 2024;301:117325. https://doi.org/10.1016/j.engstruct.2023.117325.

[20] United Nations, Department of Economic and Social Affairs. Transforming our World: The 2030 Agenda for Sustainable Development. United Nations; 2015.

[21] Gorse C, Drotleff O-B. Guide to Sustainability in the Built Environment. Berkshire: CIOB; 2023.

[22] Sultana P, Youssef MA. Seismic Performance of Modular Steel-Braced Frames Utilizing Superelastic Shape Memory Alloy Bolts in the Vertical Module Connections. Journal of Earthquake Engineering 2018;24:628–52. https://doi.org/10.1080/13632469.2018.1453394.

[23] Wu CX, Yang Y, Wu CY, Yang T, Xu X. Research on seismic behaviour analysis of shock absorbing structure and connecting joints of container assembly structures. Steel Construction 2019;34:1-8+73.

[24] Sendanayake SV, Thambiratnam DP, Perera NJ, Chan THT, Aghdamy S. Enhancing the lateral performance of modular buildings through innovative inter-modular connections. Structures 2021;29:167–84. https://doi.org/10.1016/j.istruc.2020.10.047.

[25] Jing J, Clifton GC, Roy K, Lim JBP. Seismic protection of modular buildings with galvanised steel wall tracks and bonded rubber units: Experimental and numerical study. Thin-Walled Structures 2021;162. https://doi.org/10.1016/j.tws.2021.107563.

[26] Batukan MB, Sanches R, Hashemi A, Mercan O, Fathieh A, Quenneville P. Seismic performance of modular steel buildings (MSBs) equipped with resilient slip friction joints (RSFJs). Journal of Building Engineering 2022;47:103881. https://doi.org/10.1016/j.jobe.2021.103881.

[27] Wu G, Feng D-C, Wang C-L. Modularized Suspended Building Structure. Novel Precast Concrete Structure Systems, Singapore: Springer Nature Singapore; 2023, p. 273–325. https://doi.org/10.1007/978-981-19-6821-1_8.

[28] Zhang G, Xu L, Li Z. Development and Experimental Verification of Self-Centering Haunched Plug-In Modular Connections. J Struct Eng 2023;149:04023047. https://doi.org/10.1061/JSENDH.STENG-12029.

[29] Corfar D-A, Tsavdaridis KD. A hybrid inter-module connection for steel modular building systems with SMA and high-damping rubber components. Engineering Structures 2023;289:116281. https://doi.org/10.1016/j.engstruct.2023.116281.

[30] Ahmadi H, Kingston J, Muhr AH. Dynamic Properties of Filled Rubber - Part I: Simple Model, Experimental Data and Simulated Results. Rubber Chemistry and Technology 2008;81:1–18. https://doi.org/10.5254/1.3548196.

[31] Lindley PB, Gough J. Engineering Design with Natural Rubber. 6th ed. Bertford: Tun Abdul Razak Research Centre; 2015.

[32] Lacey AW, Chen W, Hao H. Experimental methods for inter-module joints in modular building structures – A state-of-the-art review. Journal of Building Engineering 2022;46:103792. https://doi.org/10.1016/j.jobe.2021.103792.

[33] AISC. Seismic Provisions for Structural Steel Buildings. Chicago: American Institute of Steel Construction; 2022.

[34] SAC Joint Venture. Recommended Seismic Design Criteria for New Steel Moment-Frame Buildings. Federal Emergency Management Agency; 2000.

[35] Chen Z, Liu J, Yu Y, Zhou C, Yan R. Experimental study of an innovative modular steel building connection. Journal of Constructional Steel Research 2017;139:69–82. https://doi.org/10.1016/j.jcsr.2017.09.008.

[36] Sanches R, Mercan O, Roberts B. Experimental investigations of vertical post-tensioned connection for modular steel structures. Engineering Structures 2018;175:776–89. https://doi.org/10.1016/j.engstruct.2018.08.049.

[37] Zhai S-Y, Lyu Y-F, Cao K, Li G-Q, Wang W-Y, Chen C. Experimental study on bolted-cover plate corner connections for column-supported modular steel buildings. Journal of Constructional Steel Research 2022;189:107060. https://doi.org/10.1016/j.jcsr.2021.107060.

[38] BSI. Eurocode 3: Design of steel structures - Part 1-8: Design of joints. London: BSI; 2010.